ELSEVIER

Computer Methods in Applied Mechanics and Engineering 124 (1995) 195–212

Computer methods in applied mechanics and engineering

A linear nonconforming finite element method for nearly incompressible elasticity and Stokes flow

Reijo Kouhia[a], Rolf Stenberg[b,*]

[a] *Faculty of Civil Engineering, Helsinki University of Technology, 02150 Espoo, Finland*

[b] *Faculty of Mechanical Engineering, Helsinki University of Technology, 02150 Espoo, Finland*

Received 22 April 1993; revised 2 June 1994

Abstract

We introduce a new triangular element for nearly incompressible elasticity and incompressible fluid flow. The method consists of conforming linear elements for one of the displacement (or velocity for flows) component and linear nonconforming elements for the other component. The element is proved to give an optimal approximation and this is also confirmed by several numerical examples.

1. Introduction

In addition to materials for which the Poisson ratio is near one half, the problem of a nearly incompressible material stems from the fact that it arises as an intermediate step in solving problems in plasticity. Computationally, a nearly incompressible material is well know to be problematic since a direct application of a standard low order finite element method cannot be used. Usually the problem is instead reformulated by introducing a new unknown, the "pressure", by which it is of the same form as a regular perturbation of the Stokes equations arising in fluid flow. To discretize by the finite element method one now uses different approximations for the deflection (velocity) and the pressure. The discretization can be defined in two ways. The traditional "Galerkin" approach consists of transfering the natural weak formulation of the problem into the subspaces. In order that the method would work, the finite element spaces have to satisfy the well known "Babuška–Brezzi" condition. The problem of selecting finite element subspaces satisfying this condition has by now been studied in great detail, cf. the recent books [2,10]. In this approach there exists a general technique of using "bubble functions" by which stable methods can be designed.

The second approach is more recent and in it the weak finite element formulation is altered to include some properly weighted residuals of the differential equations (cf. [7] and [9] for a unified error analysis). By this technique the set of finite element spaces that can be used is considerably enlarged.

In elasticity the introduction and discretization of the pressure variable is usually just an intermediate step in order to obtain a working method; one uses discontinuous finite elements for the pressure and hence it can be condensed in the assembling phase of the calculation. In fluid flow the same approach is also very common and there the pressure elimination is made possible by a small perturbation of the incompressible condition, cf. [2,10] and Eqs. (25) and (26) below.

* Corresponding author.

SSDI 0045-7825(95)00829-2

For the two dimensional problem the two techniques mentioned above yield stable conforming elements of every degree except the lowest, i.e. linear or bilinear displacements combined with a piecewise constant pressure. However, even if it is not stable, the quadrilateral bilinear/constant element works quite well: for a wide class of meshes it has been shown to be optimally convergent provided the pressure has been smoothed in the right way, cf. [14]. For more general meshes the question of the convergence is open and hence no general smoothing procedure for the pressure is known. Therefore the element cannot be recommended for general use. The triangular element with a linear displacement (and hence a constant pressure) is well known to "lock" except in the case when the mesh is obtained from a quadrilateral mesh by drawing the two diagonals to each quadrilateral. For this type of triangulations the method behaves essentially as the quadrilateral bilinear/constant element, cf. [2, pp. 229–231]. That the pressure should be filtered can be seen from the Poiseuille flow example in Section 3 below.

In the pioneering paper [4] Crouzeix and Raviart showed that a linear/constant combination could be used for the Stokes problem with Dirichlet boundary conditions provided that the linear elements for the velocity are nonconforming, i.e. continuous only at the midpoints of the element edges. Recently a similar element for quadrilaterals has been introduced by Rannacher and Turek [15]. This approach will not, however, work for the equations of linear elasticity or the Stokes equations with certain "outflow" boundary conditions. The reason being that it leads to an element suffering from unphysical mechanisms. This question will be discussed in Section 2 below.

The purpose of this paper is to introduce a simple, but appearently new, idea: a plane elasticity element in which linear conforming elements are used for one of the displacement components and linear nonconforming elements for the other component. This means that the pressure is approximated with piecewise constants. We will prove that the method gives optimally convergent approximations for all variables independent of the Poisson ratio. For Stokes problem with Dirichlet boundary conditions it also has the advantage over the method by Crouzeix and Raviart that it asymptotically has only two thirds the number of degrees of freedom for the same mesh.

In the next section we will define our element. We then, in Section 3, give the results of some numerical calculations with the element. The last section is devoted to the mathematical stability and error analysis.

2. The finite element method

Let us recall the plain strain problem. By the principle of virtual work the displacement of the body is determined as follows: find $\boldsymbol{u} = (u_1, u_2) \in \boldsymbol{U}(\Omega)$ such that

$$2G \int_\Omega \left[\boldsymbol{\varepsilon}(\boldsymbol{u}) : \boldsymbol{\varepsilon}(\boldsymbol{v}) + \left(\frac{\nu}{1-2\nu} \right) \operatorname{div} \boldsymbol{u} \operatorname{div} \boldsymbol{v} \right] \mathrm{d}\Omega = \int_\Omega \boldsymbol{f} \cdot \boldsymbol{v} \, \mathrm{d}\Omega + \int_{\Gamma_N} \boldsymbol{g} \cdot \boldsymbol{v} \, \mathrm{d}\gamma \qquad \forall \boldsymbol{v} \in \boldsymbol{U}(\Omega). \tag{1}$$

Here $\boldsymbol{U}(\Omega)$ denotes the set of admissible displacements:

$$\boldsymbol{U}(\Omega) = \left\{ \boldsymbol{v} \in [H^1(\Omega)]^2 | \boldsymbol{v}_{|\Gamma_D} = \boldsymbol{0} \right\}. \tag{2}$$

where $\boldsymbol{f}$ is the body load and $\boldsymbol{g}$ is the traction given along the part Γ_N of the boundary of Ω. On the complementary part $\Gamma_D = \partial\Omega \setminus \Gamma_N$ of the boundary we assume that the body is fixed. Naturally, we assume that the length of Γ_D is positive. G denotes the shear modulus and ν is the Poisson ratio. We recall that $0 \leqslant \nu < \frac{1}{2}$ with the upper limit corresponding to a completely incompressible material. We further use the standard notation

$$\nabla \boldsymbol{v} = \left\{ \frac{\partial v_i}{\partial x_j} \right\}, \qquad \boldsymbol{\varepsilon}(\boldsymbol{v}) = \tfrac{1}{2} \left[\nabla \boldsymbol{v} + (\nabla \boldsymbol{v})^{\mathrm{t}} \right],$$

$$\operatorname{div} \boldsymbol{v} = \frac{\partial v_1}{\partial x_1} + \frac{\partial v_2}{\partial x_2} \quad \text{and} \quad \boldsymbol{\kappa} : \boldsymbol{\tau} = \sum_{i,j=1}^{2} \kappa_{ij} \tau_{ij}.$$

Let us also recall that the stress is given by

$$\boldsymbol{\sigma} = 2G \left(\boldsymbol{\varepsilon}(\boldsymbol{u}) + \left(\frac{\nu}{1-2\nu} \right) \operatorname{div} \boldsymbol{u} \boldsymbol{I} \right), \tag{3}$$

with $\boldsymbol{I}$ denoting the identity tensor.

Our element can now be defined as follows. We introduce a triangulation $\mathcal{C}_h$ of $\bar{\Omega}$ in the usual way and define $\boldsymbol{U}_h = (U_{1,h}, U_{2,h})$ by

$$\begin{aligned} U_{1,h} =& \{v | v \text{ is linear in every triangle of } \mathcal{C}_h, \text{ continuous at midpoints of interelement boundaries, and} \\ & \text{vanishes at the midpoints of the edges lying on } \Gamma_D\}, \\ U_{2,h} =& \{v | v \text{ is continuous in } \Omega, \text{ linear in every triangle of } \mathcal{C}_h, \text{ and vanishes on } \Gamma_D\}. \end{aligned} \tag{4}$$

We note that the degrees of freedom for this element are the following: the values of the first displacement component at the midpoints of the edges and the values of the second component at the vertices of the triangle.

The method is then: find $\boldsymbol{u}_h \in \boldsymbol{U}_h$ such that

$$2G \sum_{K \in \mathcal{C}_h} \int_K \left[\boldsymbol{\varepsilon}(\boldsymbol{u}_h) : \boldsymbol{\varepsilon}(\boldsymbol{v}) + \left(\frac{\nu}{1-2\nu} \right) \operatorname{div} \boldsymbol{u}_h \operatorname{div} \boldsymbol{v} \right] \mathrm{d}\Omega = \int_\Omega \boldsymbol{f} \cdot \boldsymbol{v} \, \mathrm{d}\Omega + \int_{\Gamma_N} \boldsymbol{g} \cdot \boldsymbol{v} \, \mathrm{d}\gamma \qquad \forall \boldsymbol{v} \in \boldsymbol{U}_h. \tag{5}$$

We remark that the method is nonconforming, i.e. it holds $\boldsymbol{U}_h \not\subset \boldsymbol{U}(\Omega)$, and hence we above have to take the sum of integrals over each element. By the same reason the approximate stress have to be defined from

$$\boldsymbol{\sigma}_{h|K} = 2G \left(\boldsymbol{\varepsilon}(\boldsymbol{u}_h) + \left(\frac{\nu}{1-2\nu} \right) \operatorname{div} \boldsymbol{u}_h \boldsymbol{I} \right)_{|K} \qquad \forall K \in \mathcal{C}_h. \tag{6}$$

We point out that the element stiffness matrix is obtained exactly by a one point integration and also that it is related to that of the standard "constant strain triangle" by a simple tranformation of the degrees of freedom.

For small values of the Poisson ratio the error analysis can be done directly for the formulation (5). Using the discrete Korn inequality proved in Lemma 4.5 below this is standard (cf. [3]), and hence in our error analysis we will only consider the problem with the Poisson ratio lying in the range, say, $\frac{1}{4} \leqslant \nu < \frac{1}{2}$. The error analysis will be based on Herrmann's formulation of (1) obtained by taking

$$p = -\left(\frac{2G\nu}{1-2\nu} \right) \operatorname{div} \boldsymbol{u} \tag{7}$$

as an independent unknown: find $\boldsymbol{u} \in \boldsymbol{U}(\Omega)$ and $p \in L^2(\Omega)$ such that

$$\begin{aligned} & 2G \int_\Omega \boldsymbol{\varepsilon}(\boldsymbol{u}) : \boldsymbol{\varepsilon}(\boldsymbol{v}) \, \mathrm{d}\Omega - \int_\Omega p \operatorname{div} \boldsymbol{v} \, \mathrm{d}\Omega = \int_\Omega \boldsymbol{f} \cdot \boldsymbol{v} \, \mathrm{d}\Omega + \int_{\Gamma_N} \boldsymbol{g} \cdot \boldsymbol{v} \, \mathrm{d}\gamma \qquad \forall \boldsymbol{v} \in \boldsymbol{U}(\Omega), \\ & \left(\frac{1-2\nu}{2G\nu} \right) \int_\Omega pq \, \mathrm{d}\Omega + \int_\Omega \operatorname{div} \boldsymbol{u} q \, \mathrm{d}\Omega = 0 \qquad \forall q \in L^2(\Omega). \end{aligned} \tag{8}$$

Next, we note that the discrete problem (5) can as well be written in a mixed form: find $\boldsymbol{u}_h \in \boldsymbol{U}_h$ and $p_h \in P_h$ such that

$$\begin{aligned} & 2G \sum_{K \in \mathcal{C}_h} \int_K \boldsymbol{\varepsilon}(\boldsymbol{u}_h) : \boldsymbol{\varepsilon}(\boldsymbol{v}) \, \mathrm{d}\Omega - \sum_{K \in \mathcal{C}_h} \int_K p_h \operatorname{div} \boldsymbol{v} \, \mathrm{d}\Omega = \int_\Omega \boldsymbol{f} \cdot \boldsymbol{v} \, \mathrm{d}\Omega + \int_{\Gamma_N} \boldsymbol{g} \cdot \boldsymbol{v} \, \mathrm{d}\gamma \qquad \forall \boldsymbol{v} \in \boldsymbol{U}_h, \\ & \left(\frac{1-2\nu}{2G\nu} \right) \int_\Omega p_h q \, \mathrm{d}\Omega + \sum_{K \in \mathcal{C}_h} \int_K \operatorname{div} \boldsymbol{u}_h q \, \mathrm{d}\Omega = 0 \qquad \forall q \in P_h, \end{aligned} \tag{9}$$

with

$$P_h = \{ q \in L^2(\Omega) | q_{|K} \in P_0(K) \quad \forall K \in \mathcal{C}_h \}. \tag{10}$$

Let us stress that the introduction of the new variable is done only as a tool for the mathematical analysis; the method is intended to be implemented by (5) in which the stiffness matrix is calculated exactly with the one point rule.

With the auxiliary unknown p_h the stress can alternatively be written as

$$\boldsymbol{\sigma}_{h|K} = (2G\boldsymbol{\varepsilon}(\boldsymbol{u}_h) - p_h \boldsymbol{I})_{|K} \qquad \forall K \in \mathcal{C}_h. \tag{11}$$

The detailed error analysis of the method will be postponed to Section 4 below. We here only give the optimal error estimate that we will prove. In addition to standard notation for Sobolev space norms and seminorms (cf. [11, pp. 266–267]) we here use the seminorm

$$|\boldsymbol{v}|_{1,h}^2 = \sum_{K\in\mathcal{C}_h} |\boldsymbol{v}|_{1,K}^2 \qquad \forall \boldsymbol{v} \in \boldsymbol{U}(\Omega) + \boldsymbol{U}_h, \tag{12}$$

and the norm

$$\|\boldsymbol{v}\|_{1,h}^2 = \operatorname{area}(\Omega)^{-1} \|\boldsymbol{v}\|_0^2 + |\boldsymbol{v}|_{1,h}^2 \qquad \forall \boldsymbol{v} \in \boldsymbol{U}(\Omega) + \boldsymbol{U}_h. \tag{13}$$

Above and throughout the paper we use dimensionally correctly scaled norms.

We have to impose the following weak restriction on the meshes to be allowed.

ASSUMPTION 2.1. Let K be any triangle of $\mathcal{C}_h$ for which all three vertices lie on the boundary $\partial\Omega$ and let (n_1, n_2) be the normal to that edge of K which lies in the interior of Ω. We assume that there is a positive constant α, independent of the mesh parameter h, such that:

(AD) $|n_1| \geqslant \alpha$ *if all vertices of K lie on the boundary part Γ_D.*

(AN) $|n_2| \geqslant \alpha$ *if all vertices of K lie on the boundary part Γ_N.*

We remark that it is very easy to ensure that this assumption is valid: one constructs the mesh so that every triangle has at least one vertex in the interior of the domain.

THEOREM 2.2. Suppose that Assumption 2.1 is valid and that h is sufficiently small. Then there is a positive constant C, independent of the Poisson ratio ν, such that

$$G\|\boldsymbol{u} - \boldsymbol{u}_h\|_{1,h} + \|\boldsymbol{\sigma} - \boldsymbol{\sigma}_h\|_0 \leqslant Ch(G|\boldsymbol{u}|_2 + |\boldsymbol{\sigma}|_1). \tag{14}$$

REMARK 2.3. The assumption that h is sufficiently small is here included in order to avoid some possible extremly coarse meshes for which the uniqueness of the solution should be checked separately. If the triangulation is constructed such that every triangle has at least one vertex in the interior of the domain, then this assumption is not needed.

Above and in the sequel the same notation C will be used for different positive constants which all are independent of the Poisson ratio ν and the mesh parameter h defined as the maximum of the diameters of the elements in the mesh $\mathcal{C}_h$. In cases when it is required by the context the constants will be numbered.

We will also use a smoothing of the stress tensor by projecting it onto the space of continuous linear elements as is customary in finite element calculations, cf. [18]. We hence define

$$\boldsymbol{\Sigma}_h = \{\boldsymbol{\tau} = \{\tau_{ij}\},\ \tau_{ij} = \tau_{ji} \in C(\Omega) | \tau_{ij|K} \in P_1(K) \quad \forall K \in \mathcal{C}_h\}, \tag{15}$$

and let $\boldsymbol{\sigma}_h^* \in \boldsymbol{\Sigma}_h$ be the smoothed stress defined from

$$\int_\Omega \boldsymbol{\sigma}_h^* : \boldsymbol{\tau}\, \mathrm{d}\Omega = \int_\Omega \boldsymbol{\sigma}_h : \boldsymbol{\tau}\, \mathrm{d}\Omega \qquad \forall \boldsymbol{\tau} \in \boldsymbol{\Sigma}_h. \tag{16}$$

In general the smoothing cannot be expected to give an improved approximation, it holds

$$\|\boldsymbol{\sigma} - \boldsymbol{\sigma}_h^*\|_0 \leqslant Ch(G|\boldsymbol{u}|_2 + |\boldsymbol{\sigma}|_1), \tag{17}$$

but for a regular mesh it is though often more accurate than the original stress $\boldsymbol{\sigma}_h$.

Let us next consider the approximation of the Stokes problem in fluid mechanics. The starting point is the system of differential equations which we first recall: find the velocity $\boldsymbol{u}$ and the pressure p such that

$$\begin{aligned} -\mu\Delta\boldsymbol{u} + \nabla p &= \boldsymbol{f}, \\ \operatorname{div}\boldsymbol{u} &= 0 \qquad \text{in } \Omega, \end{aligned} \tag{18}$$

where μ is the viscosity. In most works concentrating on the numerical analysis of finite element methods for the case of Dirichlet boundary conditions along the whole boundary is considered. Without loss of generality

these are chosen homogeneous. Hence the variational formulation is taken as: find $\boldsymbol{u} \in \boldsymbol{U}(\Omega)$ and $p \in L_0^2(\Omega)$ such that

$$\mu \int_\Omega \nabla \boldsymbol{u} : \nabla \boldsymbol{v} \, \mathrm{d}\Omega - \int_\Omega p \operatorname{div} \boldsymbol{v} \, \mathrm{d}\Omega = \int_\Omega \boldsymbol{f} \cdot \boldsymbol{v} \, \mathrm{d}\Omega \qquad \forall \boldsymbol{v} \in \boldsymbol{U}(\Omega),$$

$$\int_\Omega \operatorname{div} \boldsymbol{u} q \, \mathrm{d}\Omega = 0 \qquad \forall q \in L_0^2(\Omega), \tag{19}$$

where $\boldsymbol{U}(\Omega)$ is as in (2), with $\Gamma_D = \partial\Omega$, and the pressure has been normalized to have zero mean value, i.e. it is in the space

$$L_0^2(\Omega) = \left\{ q \in L^2(\Omega) \;\middle|\; \int_\Omega q \, \mathrm{d}\Omega = 0 \right\}. \tag{20}$$

We would now like to recall that the first equation in (18) is obtained from the equilibrium equation by using the relation $2\mu \, \mathbf{div}\, \boldsymbol{\varepsilon}(\boldsymbol{u}) = \mu \Delta \boldsymbol{u}$ which holds due to the condition $\operatorname{div} \boldsymbol{u} = 0$. (Here **div** denotes the vector valued divergence operator applied to second order tensors.) The alternative variational formulation of the Stokes problem is thus: find $\boldsymbol{u} \in \boldsymbol{U}(\Omega)$ and $p \in L_0^2(\Omega)$ such that

$$2\mu \int_\Omega \boldsymbol{\varepsilon}(\boldsymbol{u}) : \boldsymbol{\varepsilon}(\boldsymbol{v}) \, \mathrm{d}\Omega - \int_\Omega p \operatorname{div} \boldsymbol{v} \, \mathrm{d}\Omega = \int_\Omega \boldsymbol{f} \cdot \boldsymbol{v} \, \mathrm{d}\Omega \qquad \forall \boldsymbol{v} \in \boldsymbol{U}(\Omega),$$

$$\int_\Omega \operatorname{div} \boldsymbol{u} q \, \mathrm{d}\Omega = 0 \qquad \forall q \in L_0^2(\Omega). \tag{21}$$

For a conforming finite element method to work it does not matter which of the formulations (19) or (21) is used. For the method of Crouzeix and Raviart with linear nonconforming approximations for both components of the velocity the situation is different. In the original work [4] the method based on the nonconforming analog of (19) (i.e. one where integrals over Ω are replaced by sums of integrals over the elements) was considered and it was shown that the method is stable and optimally convergent. If instead the nonconforming method is defined from (21) it is easily seen that "mechanisms", or "zero energy" deflection modes different from the rigid body motions, can occure, (cf. [11, pp. 250–251]). Mathematically this means that a discrete Korn inequality (of the form (41) below) does not hold. This fact has recently been proved by Falk and Morley [6].

Suppose next, that a Dirichlet condition is imposed only on a part of the boundary and suppose that the term $\int_{\Gamma_N} \boldsymbol{g} \cdot \boldsymbol{v} \, \mathrm{d}\gamma$ is added to the right hand side of the first equations in (19) and (21). This means that the boundary condition

$$(\mu \nabla \boldsymbol{u} - p\boldsymbol{I}) \cdot \boldsymbol{n} = \boldsymbol{g}, \quad \text{on } \Gamma_N, \tag{22}$$

is variationally posed in (19), whereas the condition

$$(2\mu \boldsymbol{\varepsilon}(\boldsymbol{u}) - p\boldsymbol{I}) \cdot \boldsymbol{n} = \boldsymbol{g}, \quad \text{on } \Gamma_N, \tag{23}$$

is the condition included in (21). Of these the second alternative (23) is usually considered more realistic when modeling various "outflow" conditions and hence it seems that if Dirichlet boundary conditions are not imposed along the whole boundary, a formulation based on (21) should be prefered over one based on (19). In those cases the method of Crouzeix and Raviart cannot be used. As we will show, the present nonconforming method will work. Let us therefore explicitely write it for the Stokes equations: find $\boldsymbol{u}_h \in \boldsymbol{U}_h$ and $p_h \in P_h$ such that

$$2\mu \sum_{K \in \mathcal{C}_h} \int_K \boldsymbol{\varepsilon}(\boldsymbol{u}_h) : \boldsymbol{\varepsilon}(\boldsymbol{v}) \, \mathrm{d}\Omega - \sum_{K \in \mathcal{C}_h} \int_K p_h \operatorname{div} \boldsymbol{v} \, \mathrm{d}\Omega = \int_\Omega \boldsymbol{f} \cdot \boldsymbol{v} \, \mathrm{d}\Omega + \int_{\Gamma_N} \boldsymbol{g} \cdot \boldsymbol{v} \, \mathrm{d}\gamma \qquad \forall \boldsymbol{v} \in \boldsymbol{U}_h,$$

$$\epsilon \int_\Omega p_h q \, \mathrm{d}\Omega + \sum_{K \in \mathcal{C}_h} \int_K \operatorname{div} \boldsymbol{u}_h q \, \mathrm{d}\Omega = 0 \qquad \forall q \in P_h, \tag{24}$$

with $\boldsymbol{U}_h$ and P_h given by (4) and (10), respectively. By chosing $\epsilon = 0$ above we obtain the exact discretization. In practice the penalty formulation with a small positive ϵ is often prefered since then the pressure can be locally eliminated and the discrete problem is symmetric and positively definite in the unknown $\boldsymbol{u}_h$:

$$2\mu \sum_{K\in\mathcal{C}_h} \int_K \boldsymbol{\varepsilon}(\boldsymbol{u}_h) : \boldsymbol{\varepsilon}(\boldsymbol{v})\, \mathrm{d}\Omega + \frac{1}{\epsilon} \sum_{K\in\mathcal{C}_h} \int_K \operatorname{div} \boldsymbol{u}_h \operatorname{div} \boldsymbol{v}\, \mathrm{d}\Omega = \int_\Omega \boldsymbol{f}\cdot\boldsymbol{v}\, \mathrm{d}\Omega + \int_{\Gamma_N} \boldsymbol{g}\cdot\boldsymbol{v}\, \mathrm{d}\gamma \qquad \forall \boldsymbol{v} \in \boldsymbol{U}_h, \tag{25}$$

The pressure is then obtained by

$$p_{h|K} = -\frac{1}{\epsilon} \operatorname{div} \boldsymbol{u}_{h|K} \qquad \forall K \in \mathcal{C}_h. \tag{26}$$

Apart from the trivial notational difference in the physical constants the problem is completely equivalent to the method for the elasticity problem. Hence, we will perform the error analysis in Section 4 in the language of elasticity. For completeness we will, however, also state our main result for the case of Stokes problem.

THEOREM 2.4. Suppose that Assumption 2.1 is valid and that h is sufficiently small. If $0 \leqslant \epsilon \leqslant C_1 h^2$, *then it holds*

$$\mu \|\boldsymbol{u} - \boldsymbol{u}_h\|_{1,h} + \|p - p_h\|_0 \leqslant C_2 h(\mu |\boldsymbol{u}|_2 + |p|_1). \tag{27}$$

If the domain Ω *is convex and if* $\Gamma_D = \partial\Omega$, *we additionally have*

$$\mu \|\boldsymbol{u} - \boldsymbol{u}_h\|_0 \leqslant C_3 h^2 (\mu |\boldsymbol{u}|_2 + |p|_1). \tag{28}$$

The pressure can be smoothed by projecting onto the space of continuous piecewise linear finite elements.

Let us point out that in a triangular mesh there are assymtotically twice as many edges as vertices. Hence, our method will have approximately only two thirds as many degrees of freedom as the method of Crouzeix and Raviart.

Let us also remark that the present idea, i.e. to combine nonforming and conforming elements, could be used for quadrilateral meshes with the element of Rannacher and Turek [15]. On the other hand, for a quadrilateral mesh one could as well first divide each element into two triangles in which our element would be used. Then one can condense the degrees of freedom which are internal to each quadrilateral.

3. Numerical results

In this section we will present the results of some numerical calculations with our element. For comparison we will also give the results obtained by some other elements. As examples of elements that lock we use the linear constant strain triangle (referred to as "CST") and the bilinear element with "full integration" (QUAD). These methods are defined by (25) with the finite element subspace

$$\boldsymbol{U}_h = \{\boldsymbol{u} \in \boldsymbol{U}(\Omega) | \boldsymbol{u}_{|K} \in [R_1(K)]^2 \quad \forall K \in \mathcal{C}_h\}, \tag{29}$$

where we denote $R_1(K) = P_1(K)$ in the case when the mesh $\mathcal{C}_h$ consist of triangles and $R_1(K) = Q_1(K)$ for a quadrilateral mesh.

We also present the results obtained by the constant strain triangle for a mesh obtained by drawing the two diagonals in each element of a quadrilateral mesh (the "CST crossed mesh" method). The last method to be considered is the quadrilateral bilinear element using selective reduced integration (SRI-QUAD) defined by

$$2G \int_\Omega \left[\boldsymbol{\varepsilon}(\boldsymbol{u}_h) : \boldsymbol{\varepsilon}(\boldsymbol{v}) + \left(\frac{\nu}{1-2\nu}\right) \Pi_h \operatorname{div} \boldsymbol{u}_h \Pi_h \operatorname{div} \boldsymbol{v} \right] \mathrm{d}\Omega = \int_\Omega \boldsymbol{f}\cdot\boldsymbol{v}\, \mathrm{d}\Omega + \int_{\Gamma_N} \boldsymbol{g}\cdot\boldsymbol{v}\, \mathrm{d}\gamma \qquad \forall \boldsymbol{v} \in \boldsymbol{U}_h, \tag{30}$$

where $\boldsymbol{U}_h$ is as in (29) with $R_1(K) = Q_1(K)$ and Π_h denotes the L^2-projection onto the space of piecewise constants

$$P_h = \{q \in L^2(\Omega) | q_{|K} \in P_0(K) \quad \forall K \in \mathcal{C}_h\}. \tag{31}$$

As is well known (cf. e.g. [11]) the method is in practice implemented by a selective reduced integration. For a quite big class of meshes this method has been proved to give a convergent approximation for the displacement,

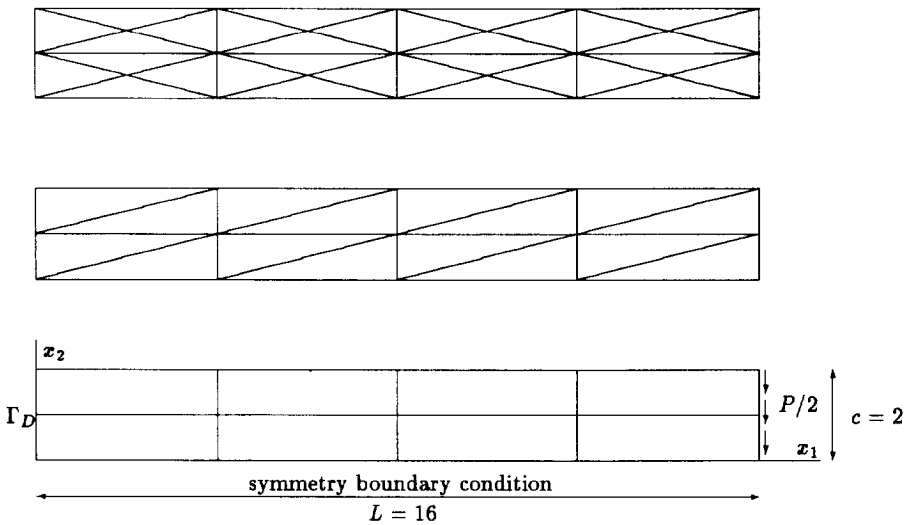

Fig. 1. Cantilever beam with parabolically varying end shear load. The 4×2 quadrilateral mesh and the corresponding triangular mesh and the crossed triangular mesh.

cf. [14]. In order that the stress would converge a filtering, as defined in [14], should be performed. In [14] the "worst case", i.e. Dirichlet conditions along the whole boundary, was considered and in practical computations this very seldom occurs. Therefore, the stress can be quite good also without the filtering. The same holds for the constant strain triangle with the crossed mesh.

For the above methods we also define a smoothed stress defined by (15) with

$$\Sigma_h = \{\boldsymbol{\tau} = \{\tau_{ij}\},\ \tau_{ij} = \tau_{ji} \in C(\Omega) | \tau_{ij|K} \in R_1(K) \quad \forall K \in \mathcal{C}_h\}. \tag{32}$$

For the bilinear element with selective reduced integration this projection is commonly used (cf. [11,18]) even if it does not exactly perform the filtering for which an analysis have been done in [14]. The projection seems, however, to perform a partial filtering but a rigorous analysis of this has not yet been presented.

EXAMPLE 3.1. A cantilever beam with a parabolic end load

This example is (a slight modification of) a standard test problem of a cantilever beam subjected to a parabolically varying end shear, cf. [11, pp. 219–255]. We let $\Omega = (0, L) \times (-c, c)$ and $\Gamma_D = \{(x_1, x_2) | x_1 = 0, x_2 \in [-c, c]\}$. On Γ_N we impose the following boundary conditions for the traction $\boldsymbol{g}$:

$$\begin{aligned} \boldsymbol{g}(x_1, \pm c) &= \boldsymbol{0}, && x_1 \in [0, L], \\ \boldsymbol{g}(L, x_2) &= \left(0,\ \frac{3P}{4c^3}\left(c^2 - x_2^2\right)\right), && x_2 \in [-c, c]. \end{aligned}$$

A standard reference solution (denoted by $\boldsymbol{u}_{\text{Ref}}$) satisfying these traction boundary conditions is

$$\begin{aligned} u_{1,\text{Ref}}(x_1, x_2) &= -\frac{P(1-\nu^2)}{4c^3 E} x_2 \left\{3\left[L^2 - (L - x_1)^2\right] + \left(\frac{2-\nu}{1-\nu}\right)\left(x_2^2 - c^2\right)\right\}, \\ u_{2,\text{Ref}}(x_1, x_2) &= \frac{P(1-\nu^2)}{4c^3 E} \left\{(L - x_1)^3 - L^3 + x_1\left[\frac{(4+\nu)c^2}{1-\nu} + 3L^2\right] + \left(\frac{3\nu}{1-\nu}\right)(L - x_1)\, x_2^2\right\}. \end{aligned} \tag{33}$$

This solution is often taken as the solution for the problem where the displacement vanish on Γ_D. We will, however, first solve the problem by imposing the exact displacement $\boldsymbol{u}_{\text{Ref}}$ on Γ_D. By symmetry only half of the domain is modelled and the data employed in the calculations are:

$$P = -1, \quad L = 16, \quad c = 2, \quad E = 1, \quad \nu = 0.3, \quad \text{and} \quad \nu = 0.499.$$

Table 1
Normalized vertical tip displacements for the cantilever beam

Element	*NEL*	*N*	$\boldsymbol{u} = \boldsymbol{u}_{\mathrm{Ref}}$ on Γ_{D}		$\boldsymbol{u} = 0$ on Γ_{D}	
			$\nu = 0.3$	$\nu = 0.499$	$\nu = 0.3$	$\nu = 0.499$
CST	16	20	0.455	0.207	0.450	0.065
	64	72	0.782	0.662	0.751	0.103
	256	272	0.933	0.733	0.918	0.213
CST crossed mesh	32	36	0.673	0.842	0.646	0.497
	128	136	0.889	0.939	0.873	0.739
	512	518	0.970	0.981	0.940	0.884
NC-CST u_1 conforming	16	36	0.882	0.884	0.884	0.908
	64	136	0.967	0.968	0.971	0.990
	256	528	0.992	0.992	0.994	1.007
NC-CST u_2 conforming	16	36	1.049	0.817	1.041	0.760
	64	136	1.023	1.023	0.999	0.876
	256	528	1.006	1.006	0.996	0.944
QUAD 2×2 int.	8	20	0.741	0.616	0.747	0.113
	32	72	0.918	0.704	0.919	0.225
	128	272	0.978	0.819	0.977	0.455
SRI-QUAD	8	20	0.756	0.842	0.737	0.708
	32	72	0.924	0.952	0.914	0.901
	128	272	0.980	0.987	0.975	0.967

In Table 1 we give the normalized tip displacement (i.e. $u_{2,h}(L,0)/u_{2,\mathrm{Ref}}(L,0)$) obtained with the finite element methods. The exact tip displacement obtained from (33) is

$$u_{2,\mathrm{Ref}}(L,0)=244.14 \quad \text{for } \nu=0.3,$$

$$u_{2,\mathrm{Ref}}(L,0)=205.74 \quad \text{for } \nu=0.499.$$

In Fig. 1 we show a quadrilateral mesh used and the corresponding triangular mesh and the crossed triangular mesh. For the nonconforming method (NC-CST) we consider both alternatives for choosing the nonconforming component of the displacement.

Next, we solve the problem by imposing the condition $\boldsymbol{u} = \boldsymbol{0}$ on Γ_{D}. For this case the exact solution is not known. Hence, we extrapolate from the results obtained with our nonconforming method for the 16×8, 32×16, 64×32 and 128×64 meshes. The values obtained are

$$u_{2,\mathrm{Extr}}(L,0)=243.29 \quad \text{for } \nu=0.3,$$

$$u_{2,\mathrm{Extr}}(L,0)=198.92 \quad \text{for } \nu=0.499.$$

In Table 1 we also give the normalized vertical displacement for this case. It is interesing to note that for the conforming linear (CST) and bilinear (QUAD) elements the locking is much more severe for this second example, whereas the methods without locking give as good results in both cases.

Since for the same mesh the methods have a different number of degrees of freedom, we in Fig. 2 give the normalized tip displacement against the number of degrees of freedom.

From Table 1 and Fig. 2 we see that our nonconforming element gives good results for this test problem.

EXAMPLE 3.2. Rigid circular inclusion in an infinite plate

We consider the case of a rigid circular inclusion of an infinite plate, subject to a unidirectional tension σ_∞. The problem definition and the computational domain is shown in Fig. 3.

The exact solutions [13] for displacements are

$$u_r = \frac{\sigma_\infty}{8Gr}\left\{(\kappa-1)r^2 + 2\gamma a^2 + \left[\beta(\kappa+1)a^2 + 2r^2 + \frac{2\delta a^4}{r^2}\right]\cos 2\theta\right\},$$

$$u_\theta = -\frac{\sigma_\infty}{8Gr}\left[\beta(\kappa-1)a^2 + 2r^2 - \frac{2\delta a^4}{r^2}\right]\sin 2\theta$$

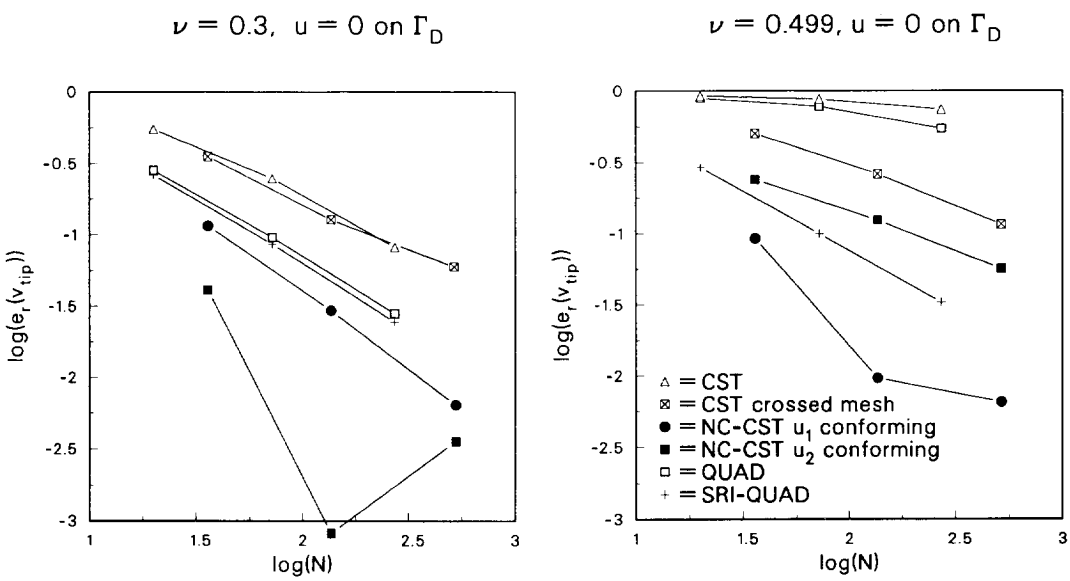

Fig. 2. Cantilever beam, convergence of tip displacement.

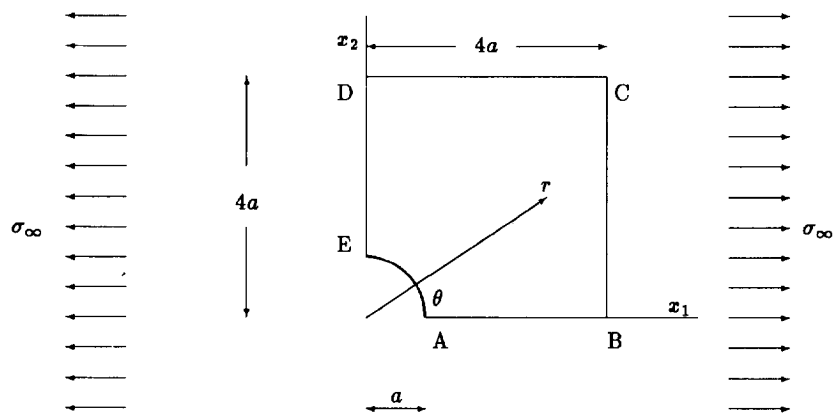

Fig. 3. Rigid circular inclusion in an infinite plate.

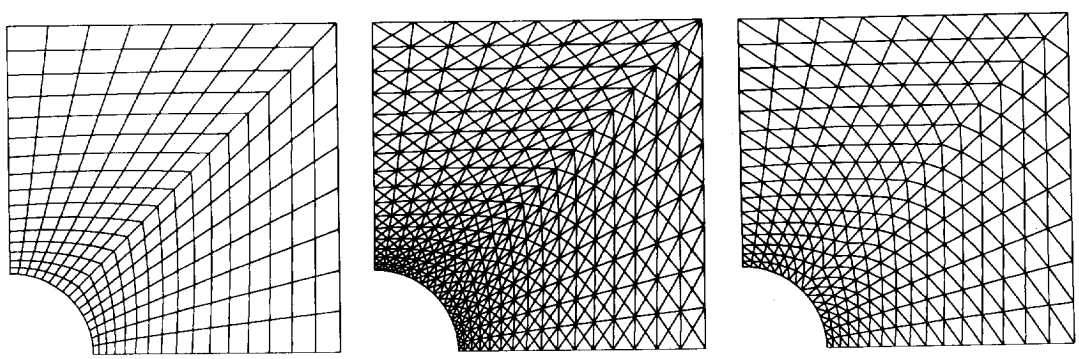

Fig. 4. The finest quadrilateral and triangular meshes used for the rigid circular inclusion.

Table 2
An infinite plate with a rigid circular inclusion; convergence of the relative L^2-errors of stresses and displacements

Element	*NEL*	*N*	$e_r(\boldsymbol{\sigma}_h)$, %	$e_r(\boldsymbol{\sigma}_h^*)$, %	$e_r(\boldsymbol{u})$, %
QUAD	4	8	>100	>100	94.45
	16	32	>100	>100	81.25
	64	128	>100	>100	52.39
	256	512	>100	>100	24.67
SRI-QUAD	4	8	23.72	14.65	8.23
	16	32	14.95	8.47	3.04
	64	128	6.69	2.82	0.71
	256	512	2.83	0.85	0.17
CST crossed	16	16	42.66	23.89	14.12
	64	64	25.44	13.86	4.65
	256	256	12.24	5.54	1.08
	1024	1024	5.33	1.79	0.25
NC-CST	8	16	21.26	19.62	7.64
	32	64	12.55	7.49	1.77
	128	256	6.61	3.08	0.52
	288	576	3.37	1.15	0.14

and stress components

$$\sigma_r = \frac{\sigma_\infty}{2}\left[1 - \frac{\gamma a^2}{r^2} + \left(1 - \frac{2\beta a^2}{r^2} - \frac{3\delta a^4}{r^4}\right)\cos 2\theta\right], \tag{34}$$

$$\sigma_\theta = \frac{\sigma_\infty}{2}\left[1 + \frac{\gamma a^2}{r^2} - \left(1 - \frac{3\delta a^4}{r^4}\right)\cos 2\theta\right], \tag{35}$$

$$\tau_{r\theta} = -\frac{\sigma_\infty}{2}\left(1 + \frac{\beta a^2}{r^2} + \frac{3\delta a^4}{r^4}\right)\sin 2\theta, \tag{36}$$

where $\kappa, \delta, \beta, \gamma$ are constants which depend on Poisson's ratio only. In our case of plane strain it holds:

$$\kappa = 3 - 4\nu, \quad \delta = \kappa^{-1}, \quad \beta = -2\delta, \quad \gamma = 2\nu - 1. \tag{37}$$

The boundary conditions imposed in the calculations are as follows: along the circular arc AE, both displacement components are zero, along the lines AB and DE symmetry conditions are imposed, and the tractions computed from (34) are given along the parts BC and CD. The Poisson ratio is $\nu = 0.4999$. Four basic quadrilateral meshes are constructed for the numerical convergence study. The meshes for the nonconforming triangular element are generated by dividing the quadrilateral elements into two triangles and the meshes for the standard linear triangle is a combination of four triangles forming the boundaries of a quadrilateral element and its diagonals, see Fig. 4. We give the results for the conforming constant strain triangle only for the "crossed meshes" since for the other triangulation the results are as bad as for the fully integrated bilinear quadrilateral element. In Table 2 we give the relative L^2-errors for the computed stress $\|\boldsymbol{\sigma} - \boldsymbol{\sigma}_h\|_0 / \|\boldsymbol{\sigma}\|_0$, the smoothed stress $\|\boldsymbol{\sigma} - \boldsymbol{\sigma}_h^*\|_0 / \|\boldsymbol{\sigma}\|_0$ and displacement $\|\boldsymbol{u} - \boldsymbol{u}_h\|_0 / \|\boldsymbol{u}\|_0$.

EXAMPLE 3.3. Cook's problem

A common test case for *plane stress* is the Cook's wing type cantilever. The problem definition is shown in Fig. 5. The physical parameters are $E = 1.0$ and $\nu = 1/3$. The cantilever is of unit thickness. We compare the behaviour of our nonconforming linear triangle only to the standard bilinear element. The left mesh in Fig. 5 is used for the case when u_2 is nonconforming. For the case when u_1 is nonconforming the assumption (AN) forces us to use the slightly modified mesh on the right. The results obtained are given in Table 3. The principal stresses at the points A and B are obtained from the post-processed stresses, as defined in (16). The results obtained with the quadrilateral method for the 128 × 128 mesh can be considered as the "exact" values.

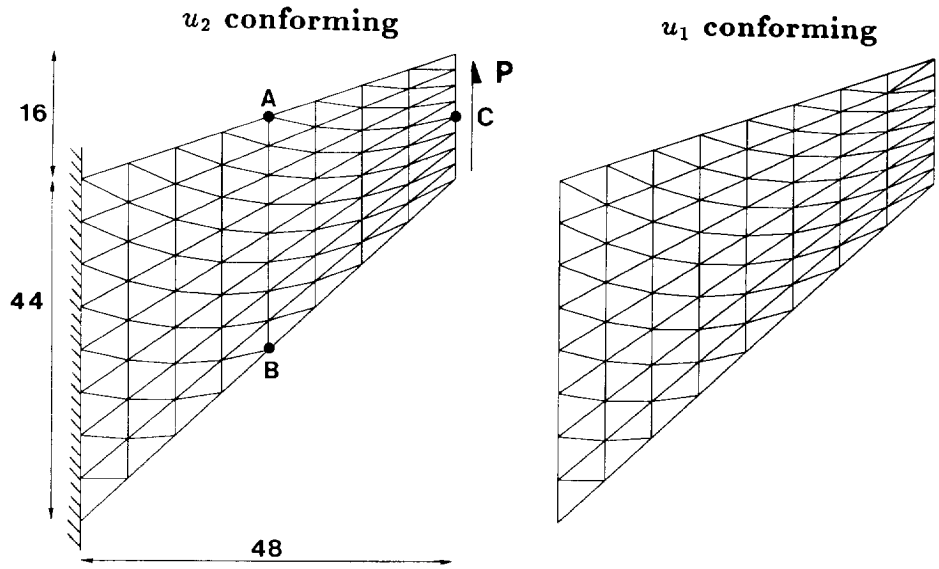

Fig. 5. Cook's cantilever problem.

Table 3
Numerical results for Cook's problem

Element	Mesh	N	$u_2(C)$	$\sigma^*_{h,\min}(A)$	$\sigma^*_{h,\max}(B)$
QUAD	2×2	12	11.85	−0.0649	0.1031
	4×4	40	18.30	−0.1382	0.1955
	8×8	144	22.08	−0.1828	0.2247
	16×16	544	23.43	−0.1986	0.2347
	32×32	2112	23.82	−0.2027	0.2370
	128×128	*33024*	*23.95*	*−0.2036*	*0.2371*
NC-CST u_1 conforming	2×2	20	20.00	−0.1662	0.1460
	4×4	72	25.46	−0.1836	0.2014
	8×8	272	23.86	−0.1920	0.2177
	16×16	1056	23.94	−0.1976	0.2268
	32×32	4160	23.94	−0.2006	0.2317
NC-CST u_2 conforming	2×2	20	31.28	−0.1126	0.2653
	4×4	72	25.51	−0.1683	0.2241
	8×8	272	24.41	−0.1833	0.2259
	16×16	1056	24.11	−0.1929	0.2301
	32×32	4160	24.01	−0.1981	0.2332

EXAMPLE 3.4. Poiseuille flow

A classical test for the Stokes problem is the Poiseuille flow, which, despite of its simplicity, reveals many unstable schemes. The same parabolic velocity profile is imposed at both the inlet and outlet of a rectangular channel. On the two other sides the velocity vanish. If H is the height of the channel the exact solution of the problem is

$$\boldsymbol{u} = (Ax_2(H - x_2), 0), \qquad p = -2\mu A x_1,$$

where A is a constant. In the computations we have chosen the domain as $\Omega = (-H, H) \times (0, H)$ with the numerical value $H = 4$. We have further chosen $2\mu A = 1/H$ so that the pressure varies from -1 to 1. The computations have been carried out both with uniform and slightly distorted meshes. The distorted meshes are constructed so that the node at the point $(-3, 3)$ in the uniform mesh is displaced to $(-2.99, 3.01)$. We use the values $\epsilon = 4.0 \cdot 10^{-5}$ and $\epsilon = 4.0 \cdot 10^{-4}$ for the penalty parameter. Three types of elements are compared: the bilinear $Q_1 - P_0$ element, the linear triangle with a crossed mesh and the new nonconforming linear triangle. The results of the computations are shown in Table 4 (here we do not use the earlier abreviations for the elements, since they are not that common within the context of fluid mechanics). The potential danger in using unstable elements is clearly seen from these results, the $Q_1 - P_0$ and the standard linear triangle yield highly

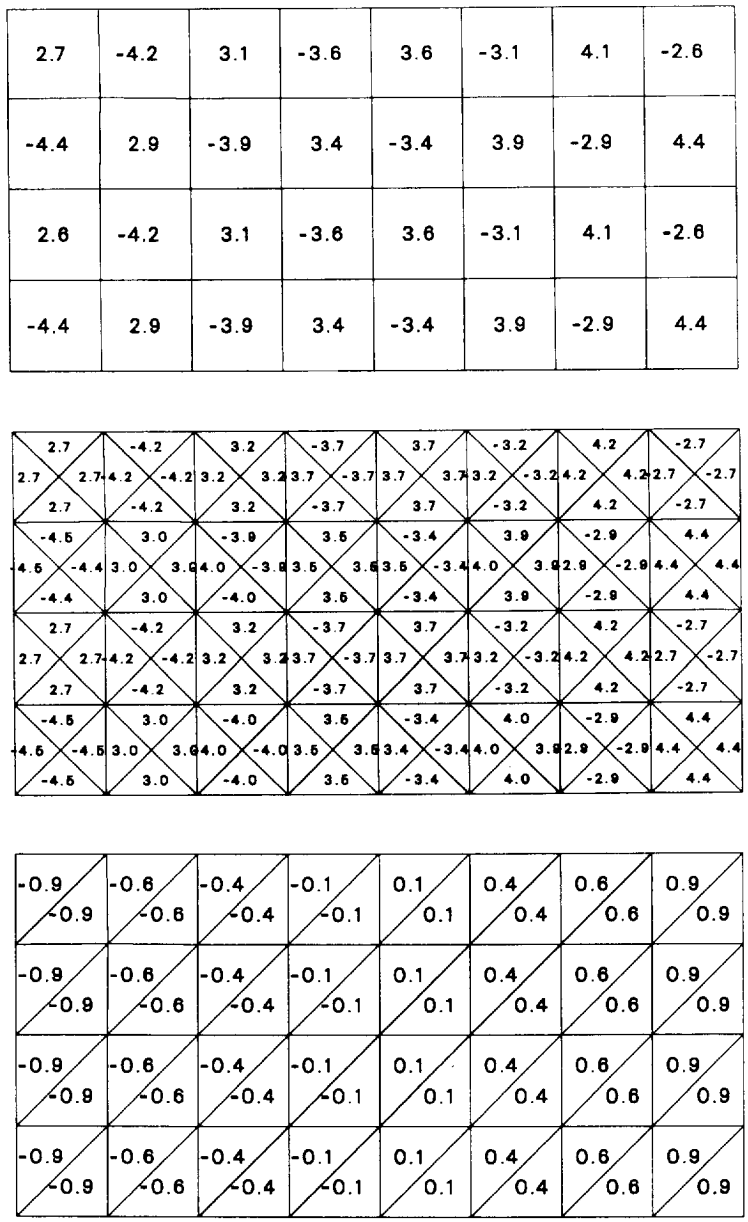

Fig. 6. Poiseuille flow, 8×4 mesh, $\epsilon = 4.0 \cdot 10^{-5}$. Pressure distribution for the $Q_1 - P_0$ element (top), linear element with a crossed mesh (middle) and the nonconforming element (bottom).

oscillatory spurious pressure modes (checkerboarding), which is seen in Fig. 6 (note the minimal distortion of the node in the upper left corner). Since we in the figure present the results with only two digits of accuracy both alternatives for the nonconforming method give the same values. This example shows that also with a crossed mesh the conforming linear element should be used cautiously for incompressible media.

4. Error analysis

We recall that in the error analysis we will restrict the Poisson ratio to lie in the interval $\frac{1}{4} \leqslant \nu < \frac{1}{2}$, as it for smaller values of ν could be done directly for the formulation (5).

Table 4
Poiseuille flow, relative L^2-error of pressure

Element	NEL	N	$\epsilon = 4.0 \cdot 10^{-5}$		$\epsilon = 4.0 \cdot 10^{-4}$	
			regular $e_r(p_h)$, %	distorted $e_r(p_h)$, %	regular $e_r(p_h)$, %	distorted $e_r(p_h)$, %
$Q_1 - P_0$	32	42	12.50	609.24	12.50	68.03
	128	210	6.25	144.58	6.25	17.74
	512	930	3.13	35.55	3.13	5.20
linear triangle crossed mesh	128	106	12.50	620.31	12.50	68.17
	512	466	6.25	146.93	6.25	17.78
	2048	1954	3.13	35.82	3.13	5.47
NC-T v_1 conforming	64	105	12.50	12.50	12.50	12.50
	256	465	6.25	6.25	6.25	6.25
	1024	1953	3.13	3.13	3.13	3.13
NC-T v_2 conforming	64	105	18.71	18.70	18.74	18.74
	256	465	9.04	9.04	9.07	9.07
	1024	1953	4.45	4.45	4.47	4.47

Let us first introduce the following abreviations:

$$\mathcal{S}(\boldsymbol{u}, p; \boldsymbol{v}, q) = 2G \sum_{K \in \mathcal{C}_h} \int_K \boldsymbol{\varepsilon}(\boldsymbol{u}) : \boldsymbol{\varepsilon}(\boldsymbol{v}) \, \mathrm{d}\Omega - \sum_{K \in \mathcal{C}_h} \int_K p \operatorname{div} \boldsymbol{v} \, \mathrm{d}\Omega - \sum_{K \in \mathcal{C}_h} \int_K \operatorname{div} \boldsymbol{u} q \, \mathrm{d}\Omega + \left(\frac{1 - 2\nu}{2G\nu} \right) \int_\Omega pq \, \mathrm{d}\Omega \tag{38}$$

and

$$|||(\boldsymbol{u}, p)|||^2 = G \|\boldsymbol{u}\|_{1,h}^2 + \frac{1}{G} \|p\|_0^2. \tag{39}$$

With this notation the discrete problem (9) is written as: find $(\boldsymbol{u}_h, p_h) \in \boldsymbol{U}_h \times P_h$ such that

$$\mathcal{S}(\boldsymbol{u}_h, p_h; \boldsymbol{v}, q) = \int_\Omega \boldsymbol{f} \cdot \boldsymbol{v} \, \mathrm{d}\Omega + \int_{\Gamma_N} \boldsymbol{g} \cdot \boldsymbol{v} \, \mathrm{d}\gamma \qquad \forall (\boldsymbol{v}, p) \in \boldsymbol{U}_h \times P_h. \tag{40}$$

Next, let us recall the main theorem of the Babuška–Brezzi saddle point theory (cf. e.g. [2,10]):

THEOREM 4.1. Suppose that the following two conditions hold:

$$\sum_{K \in \mathcal{C}_h} \int_K |\boldsymbol{\varepsilon}(\boldsymbol{v})|^2 \, \mathrm{d}\Omega \geqslant C_1 \|\boldsymbol{v}\|_{1,h}^2 \qquad \forall \boldsymbol{v} \in \boldsymbol{U}_h \tag{41}$$

and

$$\sup_{\boldsymbol{v} \in \boldsymbol{U}_h} \frac{\sum_{K \in \mathcal{C}_h} \int_K \operatorname{div} \boldsymbol{v} q \, \mathrm{d}\Omega}{\|\boldsymbol{v}\|_{1,h}} \geqslant C_2 \|q\|_0 \qquad \forall q \in P_h. \tag{42}$$

Then there is a positive constant C_3 such that

$$\sup_{(\boldsymbol{v}, q) \in \boldsymbol{U}_h \times P_h} \frac{\mathcal{S}(\boldsymbol{u}, p; \boldsymbol{v}, q)}{|||(\boldsymbol{v}, q)|||} \geqslant C_3 |||(\boldsymbol{u}, p)||| \qquad \forall (\boldsymbol{u}, p) \in \boldsymbol{U}_h \times P_h. \tag{43}$$

Let us also recall the following discrete Poincaré inequality, cf. [1, Lemma 5.3].

LEMMA 4.2. There is a positive constant C such that

$$|\boldsymbol{v}|_{1,h} \geqslant C \|\boldsymbol{v}\|_{1,h} \tag{44}$$

holds for all $\boldsymbol{v} \in \boldsymbol{U}_h$.

Of the stability conditions we will first verify the "Babuška–Brezzi" inequality.

LEMMA 4.3. Suppose that the triangulation $\mathcal{C}_h$ satisfies the assumption (AD) and that h is sufficiently small. Then the condition (42) is valid.

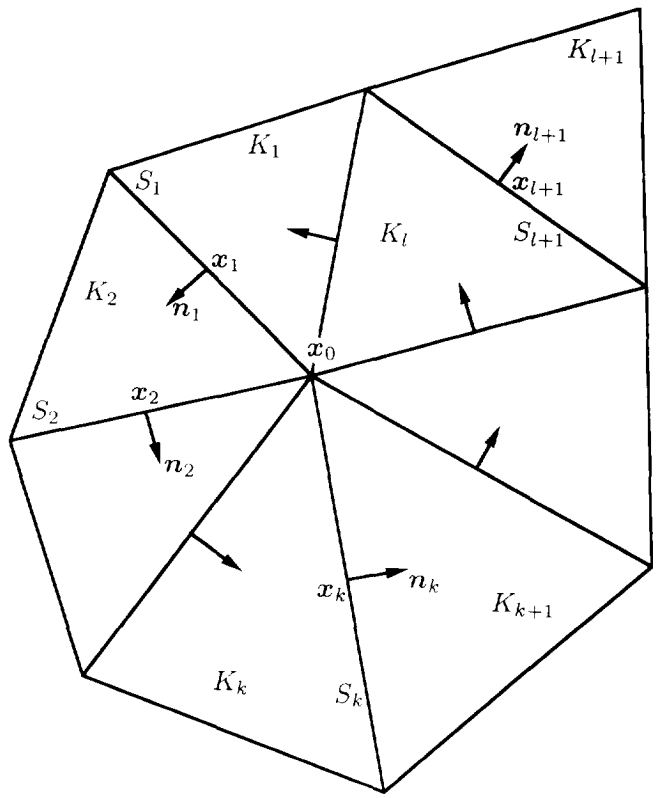

Fig. 7. Macroelements used in the proof of Lemma 4.3.

PROOF. We will use our macroelement technique as presented in [16] for conforming elements. It is, however, clear that it can be used for nonconforming elements as well.

For a macroelement M we first define

$$\boldsymbol{U}_{0,M} = \{(v_1, v_2) | (v_1, v_2)_{|K} \in [P_1(K)]^2 \quad \forall K \subset M,\ v_2 \in H_0^1(M),\ v_1 \text{ is continuous at midpoints of interelement edges and vanishes at midpoints of the edges lying on } \partial M\},$$

$$P_M = \{p | p_{|K} \in P_0(K) \quad \forall K \subset M\},$$

and

$$N_M = \left\{ p \in P_M | \sum_{K \subset M} \int_K \operatorname{div} \boldsymbol{v} p \, \mathrm{d}\Omega = 0 \quad \forall \boldsymbol{v} \in \boldsymbol{U}_{0,M} \right\}. \tag{45}$$

We will use the additional notation

$$\mathcal{N}_h = \{K \in \mathcal{C}_h | K \text{ has all three vertices on } \Gamma_N\},$$

$$\Omega_c = \bigcup_{K \in \mathcal{N}_h} K \quad \text{and} \quad \tilde{\Omega} = \Omega \setminus \Omega_c.$$

Let us organize the proof into seven steps.

Step 1. First, we consider a macroelement $M = \cup_{i=1}^{l} K_i$ consisting of triangles with one common vertex in the interior of M as in Fig. 7. For $p \in N_M$, let $p_1, p_2, \ldots, p_l$ be the constant values in the elements. In the condition that $p \in N_M$ we now choose $\boldsymbol{v} \in \boldsymbol{U}_{0,M}$ such that $v_2 \equiv 0$ and $v_1(\boldsymbol{x}_k) = 1$ and $v_1(\boldsymbol{x}_i) = 0$, $i \neq k$, $i = 1, 2, \ldots, l$, where $\boldsymbol{x}_j$ is the midpoint of the edge S_j between the triangles K_j and K_{j+1} (between K_l and K_1 when $j = l$). This gives

$$0 = \sum_{K\subset M} \int_K \operatorname{div} \boldsymbol{v} p \, \mathrm{d}\Omega = \sum_{K\subset M} \int_{\partial K} \boldsymbol{v}\cdot \boldsymbol{n} p \, \mathrm{d}\gamma = n_{1,k} \operatorname{length}(S_k)(p_k - p_{k+1}),$$

where $\boldsymbol{n}_k = (n_{1,k}, n_{2,k})$ is the normal to S_k, cf. Fig. 7. Hence, for $p \in N_M$ we have $p_k = p_{k+1}$ if $n_{1,k} \neq 0$. Since k is arbitrary, we conclude that N_M is at most two dimensional and that this happens when two edges are parallel to the x_1-axis. But choosing $\boldsymbol{v} = (0, v_2)$ with $v_2(\boldsymbol{x}_0) = 1$ (by the boundary conditions imposed all other degrees of freedom for v_2 vanish) the condition that $p \in N_M$ implies that N_M consists only of the pressures that are constant on the whole of M. This holds independent of the geometry of the macroelement and hence the local stability estimate (cf. [16]) used in the macroelement analysis holds with a constant independent of the particular macroelement of this type, i.e.

$$\sup_{v\in U_{0,M}} \frac{\sum_{K\subset M} \int_K \operatorname{div} \boldsymbol{v} q \, \mathrm{d}\Omega}{|\boldsymbol{v}|_M} \geqslant C\, |q|_M \qquad \forall q \in P_M, \tag{46}$$

with

$$|\boldsymbol{v}|_M^2 = \sum_{K\subset M} |\boldsymbol{v}|_{1,K}^2 \quad \text{and} \quad |q|_M^2 = \sum_{S\in \Gamma_M} h_S \int_S |[\![q]\!]|^2 \, \mathrm{d}\gamma,$$

where Γ_M denotes the collection of interelement edges in the interior of M and $[\![q]\!]$ is the jump in q along an edge.

Step 2. Next, we consider a macroelement $M = \cup_{i=1}^{l+1} K_i$ obtained by adjoining one element to the type of macroelement already considered, cf. Fig. 7. From Step 1 we already know that for $p \in N_M$ it holds $p_1 = p_2 = \cdots = p_l$. By chosing $\boldsymbol{v}$ such that the only nonvanishing degree of freedom is $v_1(\boldsymbol{x}_{l+1})$, where $\boldsymbol{x}_{l+1}$ is the midpoint of the edge S_{l+1} between K_l and K_{l+1}, we conclude that for $p \in N_M$ it also holds $p_l = p_{l+1}$ if $n_{1,l+1} \neq 0$, where $\boldsymbol{n}_{l+1} = (n_{1,l+1}, n_{2,l-1})$ is the normal to S_{l+1}. By restricting the possible macroelements to those for which $|n_{1,l+1}| \geqslant \alpha$, with $\alpha > 0$ fixed, one can show by a scaling type argument (cf. [16, Lemma 4]) that the local stability estimate (46) is valid with a uniform constant independent of the particular macroelement of this type.

Step 3. Let $p \in P_h$ be arbitrary and write

$$p = p^* + \overline{p} + \hat{p}, \text{ with } p_{|\Omega_c} = \hat{p}_{|\Omega_c}, \quad p_{|\widetilde{\Omega}} = (p^* + \overline{p})_{|\widetilde{\Omega}}, \tag{47}$$

(i.e. $\hat{p}_{|\widetilde{\Omega}} = 0$ and $(p^* + \overline{p})_{|\Omega_c} = 0$), $p^* \in L_0^2(\widetilde{\Omega})$ and

$$\overline{p}_{|\widetilde{\Omega}} = \frac{1}{\operatorname{area}(\widetilde{\Omega})} \int_{\widetilde{\Omega}} p \, \mathrm{d}\Omega.$$

Note that we have

$$\|p\|_0^2 = \|p^*\|_0^2 + \|\overline{p}\|_0^2 + \|\hat{p}\|_0^2. \tag{48}$$

Step 4. Now the region $\widetilde{\Omega}$ can be covered with macroelements of the types considered in Steps 1 and 2 in such a way that each element in $\widetilde{\Omega}$ belongs to at least one macroelement and each interelement boundary in $\widetilde{\Omega}$ is in the interior of at least one macroelement. For these macroelements we proved that the spaces N_M consist of the constant functions. By the macroelement technique of [16] the method defined on $\widetilde{\Omega}$ with (approximate) Dirichlet boundary conditions and a pressure in $L_0^2(\widetilde{\Omega})$ is stable. Alternatively stated: there exists $\boldsymbol{v}^* \in \boldsymbol{U}_h$ such that

$$\sum_{K\in\mathcal{C}_h} \int_K \operatorname{div} \boldsymbol{v}^* p \, \mathrm{d}\Omega = \sum_{K\in\mathcal{C}_h} \int_K \operatorname{div} \boldsymbol{v}^* p^* \, \mathrm{d}\Omega \geqslant C_1 \|p^*\|_0^2 \quad \text{and} \quad |\boldsymbol{v}^*|_{1,h} = \|p^*\|_0. \tag{49}$$

Step 5. Next, since $\Gamma_N \neq \emptyset$ it is clear that the pressure which is constant on $\widetilde{\Omega}$ can be stabilized with a function which vanish outside of $\widetilde{\Omega}$ if h is sufficiently small: there exists $\overline{\boldsymbol{v}} \in \boldsymbol{U}_h$ such that

$$\sum_{K\in\mathcal{C}_h} \int_K \operatorname{div} \overline{\boldsymbol{v}}\overline{p} \, \mathrm{d}\Omega \geqslant C_2 \|\overline{p}\|_0^2, \quad |\overline{\boldsymbol{v}}|_{1,h} = \|\overline{p}\|_0 \quad \text{and} \quad \sum_{K\in\mathcal{C}_h} \int_K \operatorname{div} \overline{\boldsymbol{v}}\hat{p} \, \mathrm{d}\Omega = 0. \tag{50}$$

Using the above relations, the Bunyakowsky–Schwarz inequality and the elementary inequality $2ab \leqslant ca^2 + b^2/c$, $a, b, c > 0$, we then get

$$\sum_{K\in\mathcal{C}_h}\int_K \operatorname{div}\overline{\boldsymbol{v}}p\,\mathrm{d}\Omega = \sum_{K\in\mathcal{C}_h}\int_K \operatorname{div}\overline{\boldsymbol{v}}(p^*+\overline{p})\,\mathrm{d}\Omega \geqslant \sum_{K\in\mathcal{C}_h}\int_K \operatorname{div}\overline{\boldsymbol{v}}p^*\,\mathrm{d}\Omega + C_2\,\|\overline{p}\|_0^2$$

$$\geqslant -C_3\,|\overline{\boldsymbol{v}}|_{1,h}\,\|p^*\|_0 + C_2\,\|\overline{p}\|_0^2 \geqslant -\frac{C_3^2}{2C_2}\,\|p^*\|_0^2 + \frac{C_2}{2}\,\|\overline{p}\|_0^2. \quad (51)$$

Step 6. For $E \in \mathcal{N}_h$ let $\boldsymbol{n}_E$ be the unit outward normal to ∂E. Define $\hat{\boldsymbol{v}} \in \boldsymbol{U}_h \cap [H^1(\Omega)]^2$ as the conforming piecewise linear function such that for each $E \in \mathcal{N}_h$ we have $\hat{\boldsymbol{v}}\cdot\boldsymbol{n}_E = h_E\hat{p}_{|E}$ (we recall that h_E is the diameter of E) along the edge of E which lies in the interior of Ω, and such that all other degrees of freedom vanish. Since the elements are regular (in the usual sense, cf. [3]) and by assuming that h is small enough, we have

$$\sum_{K\in\mathcal{C}_h}\int_K \operatorname{div}\hat{\boldsymbol{v}}\hat{p}\,\mathrm{d}\Omega \geqslant C_4\,\|\hat{p}\|_0^2 \quad \text{and} \quad |\hat{\boldsymbol{v}}|_{1,h} \leqslant C_5\,\|\hat{p}\|_0. \quad (52)$$

In the same way as in Step 5 we now obtain the estimate

$$\sum_{K\in\mathcal{C}_h}\int_K \operatorname{div}\hat{\boldsymbol{v}}p\,\mathrm{d}\Omega \geqslant -C_6(\|p^*\|_0^2 + \|\overline{p}\|_0^2) + C_7\,\|\hat{p}\|_0^2. \quad (53)$$

Step 7. With $\boldsymbol{v} = \boldsymbol{v}^* + \delta\overline{\boldsymbol{v}} + \delta^2\hat{\boldsymbol{v}}$, (49), (51), (53) and (48) give

$$\sum_{K\in\mathcal{C}_h}\int_K \operatorname{div}\boldsymbol{v}p\,\mathrm{d}\Omega \geqslant \left(C_1 - \frac{\delta C_3^2}{2C_2} - \delta^2 C_6\right)\|p^*\|_0^2 + \delta\left(\frac{C_2}{2} - \delta C_6\right)\|\overline{p}\|_0^2 + \delta^2 C_7\,\|\hat{p}\|_0^2 \geqslant C_8\,\|p\|_0^2 \quad (54)$$

when $\delta > 0$ is small enough. From the Poincaré inequality of Lemma 4.2, (49), (50) and (52) we get

$$\|\boldsymbol{v}\|_{1,h} \leqslant C_9\,\|p\|_0. \quad (55)$$

The inequalities (54) and (55) now give the asserted stability estimate. □

For the proof of the discrete Korn inequality (41) we will use a technique introduced by Falk [5]. In the proof we will need the following result proved in [16, Section 4]. Here we introduce the finite element space

$$\boldsymbol{V}_h = \left\{\boldsymbol{v} = (v_1, v_2) \in [C(\Omega)]^2 | v_{1|K} \in P_1(K),\ v_{2|K} \in P_2(K) \quad \forall K \in \mathcal{C}_h,\ \boldsymbol{v}_{|\Gamma_N} = \boldsymbol{0}\right\}. \quad (56)$$

LEMMA 4.4. Suppose that the triangulation $\mathcal{C}_h$ satisfies the assumption (AN) and that h is sufficiently small. Then there is a positive constant C such that the following condition holds:

$$\sup_{v\in V_h}\frac{\int_\Omega \operatorname{div}\boldsymbol{v}q\,\mathrm{d}\Omega}{\|\boldsymbol{v}\|_1} \geqslant C\,\|q\|_0 \quad \forall q \in P_h. \quad (57)$$

PROOF. The proof is analogous to that of Lemma 4.3 above. The Steps 1–4 were done in [16]. The rest of the proof is the same as Steps 5–7 in the proof of Lemma 4.3. □

Let us next introduce some additional notation:

$$\operatorname{rot}\boldsymbol{v} = -\frac{\partial v_1}{\partial x_2} + \frac{\partial v_2}{\partial x_1}, \quad \boldsymbol{\chi} = \begin{pmatrix} 0 & -1 \\ 1 & 0 \end{pmatrix} \text{ and } \mathbf{curl}\,\boldsymbol{v} = \begin{pmatrix} \partial v_1/\partial x_2 & -\partial v_1/\partial x_1 \\ \partial v_2/\partial x_2 & -\partial v_2/\partial x_1 \end{pmatrix}.$$

We are now ready to prove the discrete Korn inequality. For completeness we will give the proof in detail even if it follows the ideas given in [5].

LEMMA 4.5. Suppose that the triangulation $\mathcal{C}_h$ satisfies the assumption (AN) and that h is sufficiently small. Then the discrete Korn inequality (41) is valid.

PROOF. For $\boldsymbol{v} \in \boldsymbol{U}_h$ arbitrary we write

$$\boldsymbol{\varepsilon}(\boldsymbol{v})_{|K} = (\nabla \boldsymbol{v} - \tfrac{1}{2} \operatorname{rot} \boldsymbol{v}\boldsymbol{\chi})_{|K} \qquad \forall K \in \mathcal{C}_h. \tag{58}$$

By Lemma 4.3 we know that there exists $z \in \boldsymbol{V}_h$ satisfying

$$\int_\Omega \operatorname{div} z q \, \mathrm{d}\Omega = \sum_{K \in \mathcal{C}_h} \int_K \operatorname{rot} \boldsymbol{v} q \, \mathrm{d}\Omega \qquad \forall q \in P_h, \tag{59}$$

and

$$|z|_1 \leqslant C \, |\boldsymbol{v}|_{1,h}. \tag{60}$$

Next, we define $\boldsymbol{\tau}$ by

$$\boldsymbol{\tau}_{|K} = (\nabla \boldsymbol{v} - \mathbf{curl}\, z)_{|K} \qquad \forall K \in \mathcal{C}_h. \tag{61}$$

Integrating by parts one obtains

$$\sum_{K \in \mathcal{C}_h} \int_K \nabla \boldsymbol{v} : \mathbf{curl}\, z \, \mathrm{d}\Omega = \sum_{K \in \mathcal{C}_h} \int_{\partial K} (v_1 \nabla z_1 \cdot \boldsymbol{t}_K + v_2 \nabla z_2 \cdot \boldsymbol{t}_K) \, \mathrm{d}\gamma, \tag{62}$$

where $\boldsymbol{t}_K$ is the counterclockwise tangent to ∂K. Now, let us inspect the different contributions to the the sum of integrals on the righthand side above. First, we recall that $z = \mathbf{0}$ on Γ_N. Hence, the contribution from the edges lying on the boundary part Γ_N vanish. Next, consider the contribution from interior edges. Let $E_{12} = K_1 \cap K_2$ be the common edge of two adjoining triangles K_1 and K_2 in $\mathcal{C}_h$. On the edge it holds

$$\nabla z_i \cdot \boldsymbol{t}_{K_1} + \nabla z_i \cdot \boldsymbol{t}_{K_2} = 0, \quad i = 1, 2. \tag{63}$$

Since the component v_2 is conforming this directly gives

$$\int_{E_{12}} v_{2|K_1} \nabla z_2 \cdot \boldsymbol{t}_{K_1} \, \mathrm{d}\gamma + \int_{E_{12}} v_{2|K_2} \nabla z_2 \cdot \boldsymbol{t}_{K_2} \, \mathrm{d}\gamma = \int_{E_{12}} v_2 (\nabla z_2 \cdot \boldsymbol{t}_{K_1} + \nabla z_2 \cdot \boldsymbol{t}_{K_2}) \, \mathrm{d}\gamma = 0. \tag{64}$$

Since $\nabla z_1 \cdot \boldsymbol{t}_{K_i}, i = 1, 2$, are constants with opposite values we get

$$\int_{E_{12}} v_{1|K_1} \nabla z_1 \cdot \boldsymbol{t}_{K_1} \, \mathrm{d}\gamma + \int_{E_{12}} v_{1|K_2} \nabla z_1 \cdot \boldsymbol{t}_{K_2} \, \mathrm{d}\gamma = \nabla z_1 \cdot \boldsymbol{t}_{K_1} \int_{E_{12}} (v_{1|K_1} - v_{1|K_2}) \, \mathrm{d}\gamma = 0, \tag{65}$$

where the last integral vanish since the integrand is a linear function vanishing at the midpoint of the edge. From (64) and (65) we see that the contribution from interior edges in the sum of integrals in the right hand side of (62) vanish. Finally, on an edge $E \subset \Gamma_D$ it holds $v_2 = 0$ and since v_1 vanish at the midpoint, and $\nabla z_1 \cdot \boldsymbol{t}_K$ (with $E = K \cap \Gamma_D$) is a constant, we have

$$\int_E (v_1 \nabla z_1 \cdot \boldsymbol{t}_K + v_2 \nabla z_2 \cdot \boldsymbol{t}_K) \, \mathrm{d}\gamma = \int_E v_1 \nabla z_1 \cdot \boldsymbol{t}_K \, \mathrm{d}\gamma = \nabla z_1 \cdot \boldsymbol{t}_K \int_E v_1 \, \mathrm{d}\gamma = 0, \tag{66}$$

i.e. the contributions to the right hand side of (62) by edges on Γ_D also vanish. We have now proved that

$$\sum_{K \in \mathcal{C}_h} \int_K \nabla \boldsymbol{v} : \mathbf{curl}\, z \, \mathrm{d}\Omega = 0. \tag{67}$$

Using this orthogonality relation, (58) and (59) we thus obtain

$$\begin{aligned} \sum_{K \in \mathcal{C}_h} \int_K \boldsymbol{\varepsilon}(\boldsymbol{v}) : \boldsymbol{\tau} \, \mathrm{d}\Omega &= \sum_{K \in \mathcal{C}_h} \int_K (\nabla \boldsymbol{v} - \tfrac{1}{2} \operatorname{rot} \boldsymbol{v}\boldsymbol{\chi}) : (\nabla \boldsymbol{v} - \mathbf{curl}\, z) \, \mathrm{d}\Omega \\ &= \sum_{K \in \mathcal{C}_h} \int_K |\nabla \boldsymbol{v}|^2 \, \mathrm{d}\Omega - \tfrac{1}{2} \sum_{K \in \mathcal{C}_h} \int_K \operatorname{rot} \boldsymbol{v} (\operatorname{rot} \boldsymbol{v} - \operatorname{div} z) \, \mathrm{d}\Omega = \sum_{K \in \mathcal{C}_h} \int_K |\nabla \boldsymbol{v}|^2 \, \mathrm{d}\Omega = |\boldsymbol{v}|_{1,h}^2. \end{aligned} \tag{68}$$

From (61) and (60) and we get

$$\|\boldsymbol{\tau}\|_0 \leqslant |\boldsymbol{v}|_{1,h} + |z|_1 \leqslant C \, |\boldsymbol{v}|_{1,h}. \tag{69}$$

The Bunyakowsky–Schwarz inequality, (68) and (69) then give

$$\Big(\sum_{K\in\mathcal{C}_h}\int_K |\boldsymbol{\varepsilon}(\boldsymbol{v})|^2\,\mathrm{d}\Omega\Big)^{\frac{1}{2}} \geqslant \sum_{K\in\mathcal{C}_h}\int_K \boldsymbol{\varepsilon}(\boldsymbol{v}) : \boldsymbol{\tau}\,\mathrm{d}\Omega / \|\boldsymbol{\tau}\|_0 \geqslant C\,|\boldsymbol{v}|_{1,h}. \tag{70}$$

The assertion now follows from Lemma 4.4. □

Let us now end the paper by sketching the

Proof of Theorems 2.2 and 2.4. From Lemmas 4.2 and 4.4, and Theorem 4.1 the stability inequality (43) is valid. By the theory of nonconforming mixed methods (cf. [2]) this implies that

$$|||(\boldsymbol{u}-\boldsymbol{u}_h, p-p_h)||| \leqslant C\left\{\inf_{(v,q)\in U_h\times P_h} |||(\boldsymbol{u}-\boldsymbol{v}, p-q)||| + \sup_{v\in U_h}\left\{\sum_{K\in\mathcal{C}_h}\int_{\partial K}((2G\boldsymbol{\varepsilon}(\boldsymbol{u})-p\boldsymbol{I})\cdot\boldsymbol{n})_1\cdot v_1\,\mathrm{d}\gamma / \|\boldsymbol{v}\|_{1,h}\right\}\right\} \tag{71}$$

with the positive constant C independent of ν. We now use standard interpolation estimates for first term in the right hand side above and for the second term we use a basic estimate for linear nonconforming methods given by Crouzeix and Raviart [4, Lemma 3]. By this we arrive at the estimate (14) (and (27)).

The L^2-estimate for the velocity for the Stokes problem with Dirichlet boundary conditions along the whole boundary is derived by the usual Aubin–Nitsche technique in which Lemma 3 of [4] is needed. □

References

[1] D.N. Arnold and R.S. Falk, A uniformly accurate finite element method for the Reissner–Mindlin plate, SIAM J. Numer. Anal. 26 (1989) 1276–1290.

[2] F. Brezzi and M. Fortin, Mixed and Hybrid Finite Element Methods (Springer-Verlag, Berlin, 1991).

[3] P.G. Ciarlet, The Finite Element Method for Elliptic Problems (North-Holland, Amsterdam, 1978).

[4] M. Crouzeix and P.A. Raviart, Conforming and nonconforming finite element methods for solving the stationary Stokes equations, RAIRO Anal. Numér. R-3 (1973) 33–76.

[5] R.S. Falk, Nonconforming finite element methods for the equations of linear elasticity. Math. Comput. 57 (1991) 529–550.

[6] R.S. Falk and M. Morley, Equivalence of finite element methods for problems in elasticity, SIAM J. Numer. Anal. 27 (1990) 1486–1505.

[7] L.P. Franca and T.J.R. Hughes, Two classes of mixed finite element methods, Comput. Methods Appl. Mech. Engrg. 69 (1988) 89–129.

[8] M. Fortin, Old and new finite elements for incompressible flows, Int. J. Numer. Methods Fluids 1 (1981) 347–364.

[9] L.P. Franca and R. Stenberg, Error analysis of some Galerkin least squares methods for the elasticity equations, SIAM J. Numer. Anal. 28 (1991) 1680–1697.

[10] V. Girault and P.A. Raviart, Finite Element Methods for Navier-Stokes Equations. Theory and Algorithms (Springer-Verlag, Berlin, 1986).

[11] T.J.R. Hughes, The Finite Element Method. Linear Static and Dynamic Analysis (Prentice-Hall, Englewood Cliffs, 1987).

[12] T.J.R. Hughes and L.P. Franca, A new finite element formulation for computational fluid dynamics: Part VII. The Stokes problem with various well-posed boundary conditions: symmetric formulations that converge for all velocity/pressure spaces, Comput. Methods Appl. Mech. Engrg. 65 (1987) 85–96.

[13] N.I. Muskhelishvili, Some Basic Problems of the Mathematical Theory of Elasticity (Noordhoff, Leiden, 1953).

[14] J. Pitkäranta and R. Stenberg, Error bounds for the approximation of Stokes problem with bilinear/constant elements on irregular quadrilateral meshes, in: J.R. Whiteman, ed., The Mathematics of Finite Elements and Applications V, MAFELAP 1984 (Academic Press, New York, 1985) 325–334.

[15] R. Rannacher and S. Turek, Simple nonconforming quadrilateral Stokes element, Numer. Methods PDE's 8 (1992) 97–112.

[16] R. Stenberg, A technique for analysing finite element methods for viscous incompressible flow, Int. J. Numer. Methods Fluids 11 (1990) 935–948.

[17] B. Szabó and I. Babuška, Finite Element Analysis (Wiley, New York, 1991).

[18] O.C. Zienkiewicz and R.L. Taylor, The Finite Element Method, 4th edition, Vol. 1 (MacGraw-Hill, New York, 1989).